

1 **A multifaceted approach to investigate interactions of thifluzamide with**
2 **haemoglobin**

3 **Sandeep Yadav,^{§,1,2} Shubham Sewariya,^{§,3,4} Anirudh Pratap Singh Raman,^{§,1,2} Arun,⁵**
4 **Prashant Singh^{1,*} Ramesh Chandra,³ Pallavi Jain,² Anju Singh,^{3,5} Kamlesh Kumari^{6,*}**
5

6 ¹Department of Chemistry, Atma Ram Sanatan Dharma College, University of Delhi, New
7 Delhi, India;

8 ²Department of Chemistry, SRM Institute of Science & Technology, Delhi-NCR Campus,
9 Modinagar, India;

10 ³Department of Chemistry, University of Delhi, Delhi, India;

11 ⁴School of Pharmacy and Biomedical Sciences, University of Central Lancashire, Preston, UK;

12 ⁵Department of Chemistry, Hindu College, University of Delhi, Delhi, India;

13 ⁶Department of Zoology, University of Delhi, Delhi, India
14
15

16 § equal authorship

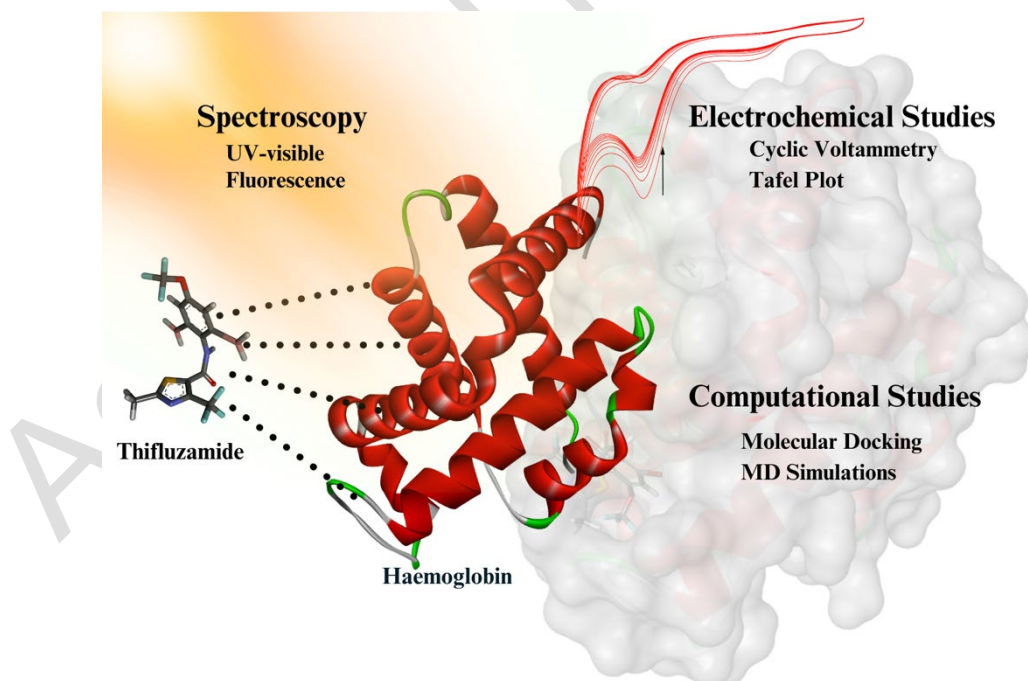
17 * Corresponding author

18 Email: psingh@arsd.du.ac.in and kkumari@zoology.du.ac.in
19
20
21
22
23
24
25
26
27
28
29
30
31
32
33
34
35
36
37
38
39
40
41

42

43 **Abstract**

44 This study explores the interaction between the pesticide thifluzamide (TF) and haemoglobin
45 (Hb) to understand potential structural changes that might affect Hb's function. Using a
46 combination of UV-visible and fluorescence spectroscopy, circular dichroism (CD), molecular
47 docking, molecular dynamics (MD) simulations, and electrochemical methods, we investigated
48 these interactions in detail. Spectroscopy results indicated the formation of a stable TF-Hb
49 complex, with a binding constant of $6.64 \times 10^5 \text{ M}^{-1}$ at 298 K and a 1:1 binding ratio. The
50 stability of this complex was confirmed by a free energy change (ΔG) of $-34.491 \text{ kJ mol}^{-1}$. CD
51 spectroscopy was employed to confirm structural changes in Hb due to thifluzamide binding.
52 Molecular docking studies revealed that TF interacts with specific amino acids in Hb, such as
53 ALA, HIS, VAL, LYS, and LEU, with a binding energy of $-25.10 \text{ kJ mol}^{-1}$. MD simulations
54 supported these findings by showing conformational changes in Hb upon TF binding, as
55 indicated by RMSD and RMSF analyses. Electrochemical experiments further confirmed the
56 interaction, evidenced by a consistent decrease in the TF peak in the presence of Hb. Overall,
57 our findings shed light on how TF binds to Hb, causing structural changes that could potentially
58 impact its normal function. This research enhances our understanding of the biochemical
59 effects of TF on Hb, which could have significant implications for biological systems.



60

61 **Keywords:** Thifluzamide, haemoglobin, cyclic voltammetry, static quenching, MD
62 simulations, circular dichroism, time resolved fluorescence spectroscopy, UV-visible
63 spectroscopy

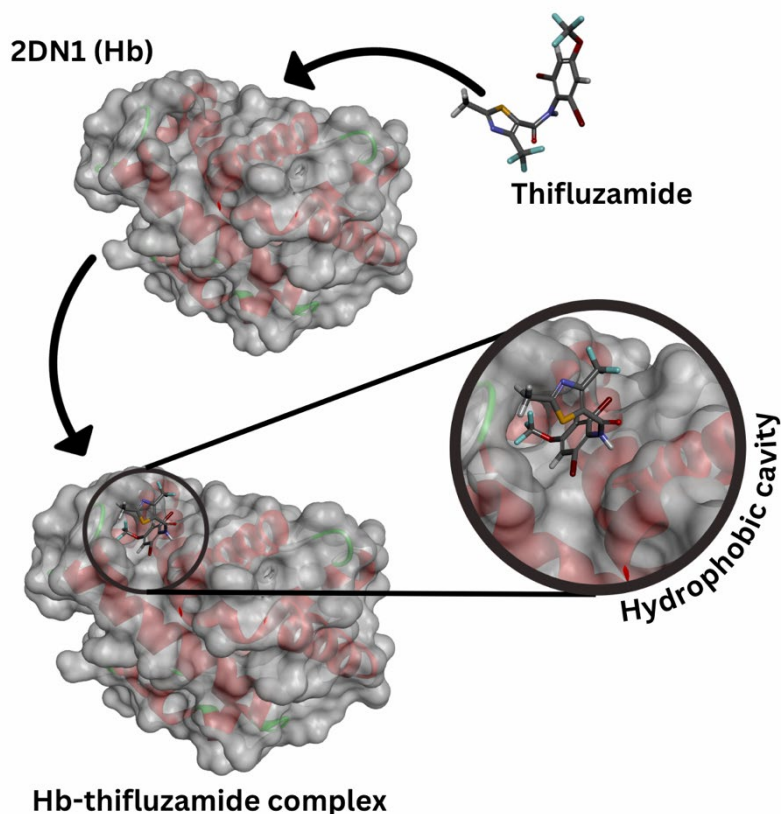
64 1. Introduction

65 The extensive use of pesticides has led to significant negative impacts on both environmental
66 and human health[1]. Pesticide residues in food and the environment can affect genetic
67 polymorphisms and lead to other illnesses[2], [3]. TF, a benzamide-class fungicide, is notable
68 not only for its efficacy in agriculture but also for its potential biological interactions. It is
69 widely used to combat sheath blight in rice fields across Asia[4], [5]. Due to its extensive
70 application, TF often enters nearby aquatic ecosystems through runoff and spray drift, raising
71 environmental concerns[6], [7]. Studies have revealed that TF persists in marine environments,
72 leading to prolonged exposure risks for aquatic organisms[8]

73 Recent studies indicate that TF interacts with biological macromolecules, raising concerns
74 about its potential health implications[9]. For instance, Yang et al. (2021) revealed that TF
75 exposure in zebrafish embryos impairs neuroendocrine function and causes developmental
76 abnormalities, suggesting significant toxicity[10]. Additionally, other studies have reported its
77 toxic effects on earthworms and soil fungal communities, indicating a broad spectrum of
78 biological impacts. Structurally, the hydrophobicity of thifluzamide primarily arises from its
79 aromatic ring and alkyl chains, which are nonpolar and tend to avoid water, contributing to the
80 compound's overall lipophilic behavior. On the other hand, large number of halogen atoms (Br
81 and F) present in its structure introduces polar characteristics, making it capable of forming
82 hydrogen bonds with water, thus imparting some hydrophilic properties. However, the
83 predominant nature of thifluzamide is hydrophobic due to the larger nonpolar components of
84 its structure[11].

85 Haemoglobin, a crucial protein in red blood cells, is essential for oxygen transport throughout
86 the body[12]. Extensive research on Hb's complex structure and functionality aims to
87 understand physiological processes better and develop clinical treatments. In Hb, hydrophobic
88 binding sites are mostly located inside the protein, helping to stabilize its structure. Key
89 residues like valine, leucine, alanine, and phenylalanine form a core that supports the heme
90 pocket, essential for oxygen binding. On the other hand, hydrophilic binding sites are found on
91 the surface, where residues such as lysine, histidine, and glutamic acid interact with water and
92 aid in solubility[13], [14]. This balance between hydrophobic and hydrophilic interactions is
93 crucial for maintaining Hb's structure and ensuring efficient oxygen transport and release.
94 Given thifluzamide's hydrophobic nature and its ability to form hydrogen bonds, it is likely
95 that the compound could interact with both the hydrophobic cavity and hydrophilic surface of
96 Hb as illustrated in **Figure 1**. The nonpolar regions of thifluzamide may favor binding within

97 Hb's hydrophobic sites, while its halogen atoms could interact with hydrophilic residues,
98 suggesting a potential for stable complex formation.



99

100 **Figure 1** Illustration of thifluzamide binding to Hb at a hydrophobic cavity.

101 Previous research by our group showed that dinotefuran pesticide strongly binds to human Hb,
102 inducing conformational changes and inhibiting its function [15]. A similar study with another
103 small organic molecule was also done; interactions of Ofloxacin-Hb were investigated using
104 spectroscopic, *in-silico* and electrochemical methods[16]. Studies on other pesticides, such as
105 TEPP, imidacloprid, and paraquat, have highlighted the potential for adverse effects on Hb's
106 structure and function[17], [18]. Recent spectroscopy and computational biology
107 advancements have enhanced our understanding of ligand-protein interactions[19], [20], [21],
108 [22].

109 Understanding the interaction between TF and Hb is crucial for assessing its impact on blood
110 function, which is essential for evaluating its overall health risks. This study employs a
111 comprehensive methodology to thoroughly examine the interaction between TF and Hb,
112 including UV-visible spectroscopy, fluorescence, electrochemistry, molecular docking, and
113 molecular dynamics (MD) simulations. This multi-faceted approach provides a detailed
114 understanding of TF's effects on Hb. It contributes significantly to our knowledge of its
115 potential health risks.

116

117

118 2. Experimental

119 2.1 Materials

120 The PBS buffer capsules (Product ID-31390E) were procured from MOLYCHEM.
121 Lyophilised powder of haemoglobin human (Product ID-H7379) was obtained from MERCK.
122 Agilent Technologies Inc. provided TF with a purity of 95%.

123

124 2.2 Methodology

125 2.2.1 UV-Visible Spectroscopy

126 UV-visible Spectrophotometer of Thermo Fisher Scientific (Evolution 300) was used to
127 investigate the interaction between TF and Hb. Experiments were conducted at room
128 temperature (298 K) and a pH of 7.4. The authors recorded the absorbance at an optimised
129 constant Hb concentration of 2.5 μM and then gradually adding the drug from 0 to 320 μM .
130 The baseline in the experiment was set using a reference solution of 1X PBS buffer. Triplicate
131 study was done to ensure the accuracy of the study.

132

133 2.2.2 Fluorescence Spectroscopy

134 Hitachi F-7000 Fluorescence Spectrophotometer was used to record emission spectra for TF
135 with and without Hb. In the experiment, authors titrated TF with Hb at 298, 303 and 308 K
136 individually. Further, the molarity of TF was varied from 0 to 280 μM . For the experiment, the
137 excitation was done with 280 nm (due to more robust absorbance of aromatic amino acid
138 residues at this wavelength and it also being the consistent choice for understanding ligand-
139 protein interactions) and the emission spectra were recorded between 290 nm to 500 nm. The
140 width of slits was 5 nm, and the spectra have been taken having a scan rate of 1200 nm/ min.
141 To account for the inner filter effect and for assessment of fluorescence data, authors applied
142 the following **equation (1)**:

$$143 F_{\text{corrected}} = F_{\text{observed}} \cdot e^{(A_{\text{ex}} + A_{\text{em}})/2} \quad (1)$$

144 In the equation, F_{observed} is the observed fluorescence of Hb, $F_{\text{corrected}}$ denotes the corrected
145 fluorescence upon considering the inner filter effect. A_{ex} and A_{em} are the absorption of TF at
146 excitation and emission wavelengths, respectively.

147 For time resolved fluorescence study, 5 μM Hb solution was prepared by dissolving Hb in a
148 buffer solution, ensuring a consistent concentration throughout the experiment. Thifluzamide
149 was gradually added to the Hb solution in varying concentrations (0 μM , 40 μM , 120 μM , 200

150 μM , 240 μM , 280 μM). After each addition, the solution was thoroughly mixed to ensure
151 uniform distribution. Time-resolved fluorescence (TRF) measurements were performed using
152 a single-photon counting spectrophotometer (Horiba Scientific, Delta Flex Jobin Yvon
153 technology, Glasgow, UK) with excitation at 338nm. The fluorescence decay curves were
154 recorded and analyzed to obtain the fluorescence lifetimes (Γ_1 , Γ_2 , Γ_3) and their respective
155 amplitudes (α_1 , α_2 , α_3).

156

157 **2.2.3 Circular Dichroism Spectroscopy**

158 The structural changes in Hb upon binding with thifluzamide were investigated using Circular
159 Dichroism (CD) spectroscopy. Initially, a stock solution of 1 μM Hb was prepared in a 10mM
160 phosphate buffer at pH 7.4. Solution of thifluzamide was added to the Hb to gradually increase
161 the concentration of thifluzamide (1 μM , 2 μM , 3 μM , 4 μM , 5 μM). The CD spectra were
162 recorded in the far-UV region (190-250 nm) at room temperature using JASCO 815 CD
163 spectrophotometer. The spectra of pure Hb and the Hb-thifluzamide complexes were measured
164 to observe any changes in the secondary structure of Hb due to the binding of thifluzamide.

165

166 **2.2.4 *In silico* studies**

167 *Molecular Docking*

168 The corresponding PDB (ID: 2DN1) was obtained from the RCSB protein data bank.
169 Subsequently, the protein was prepared for docking utilising Chimera, Notepad++ and
170 Discovery Studio[20]. Initially, any existing ligands bound to the protein were removed,
171 followed by adding polar hydrogen atoms and balancing of charges. The structure of the
172 pesticide was designed using ChemDraw Professional and saved in mol2 format for further
173 analysis and docking studies[21]. Structural optimisation of the pesticide was done using the
174 Molecular Mechanics 2 (MM2) forcefield in Chem3D to minimise the energy. Further, to
175 analyse the interactions occurring between TF with various amino acids of Hb, AutoDock was
176 used to perform molecular docking. AutoDock uses an advanced computational method
177 employed in molecular modelling to anticipate the binding mode and strength between a
178 protein target and a small molecule ligand[23], [24], [25], [26], [27]. It utilises various
179 algorithms and scoring functions to navigate the ligand's conformational space within the
180 protein's binding site, aiming to identify favourable energy configurations. An exhaustiveness
181 level of 40 was utilized. The grid box dimensions were set to 20x20x20 Å, with the coordinates
182 being x=40.85, y=28.81, and z=15.95 to ensure site-specific docking. AutoDock's capability to
183 account for flexibility in both the ligand and protein enables a thorough examination of

184 potential binding modes[28], [29]. Molecular docking was performed to provide the initial pose
185 for subsequent MD simulations. This approach is a standard procedure in computational
186 studies, as MD simulations are designed to mimic actual physiological conditions.

187 *Molecular dynamics (MD) simulations*

188 To understand the behaviour of TF in water and its interactions with Hb MD simulations
189 using GROMACS was performed [30], [31], [32]. The topology of the complex was prepared
190 by applying the CHARMM27 force field, and the SPC/E-TIP3P water model was used for
191 solvation[33]. A cubic simulation box was used with dimensions of 5.883×5.883×5.883 nm,
192 resulting in a volume of 203.644 nm³. The box was solvated with 5791 water molecules. The
193 density of the system, which included the Hb-TF complex and the water molecules, was
194 calculated to be 986.233 g/L. The system was equilibrated for 500 ps for a stable configuration
195 and thermal equilibrium. NVT and NPT ensembles were also utilised to stabilise the system
196 prior to MD simulations. Simulations were run for 250 ns to ensure that statistically meaningful
197 data was collected for further analysis. Reference temperature for the simulations was kept at
198 300 K which is the default temperature of GROMACS module. Various parameters like
199 structural fluctuations, intermolecular interactions, and diffusion coefficients were monitored.
200 Trajectories obtained from the simulations were used to calculate root mean square fluctuation
201 (RMSF), Root mean square deviation (RMSD), and the number of hydrogen bonds between
202 TF and Hb [34], [35]. The data obtained from the trajectory file was plotted in OriginPro to
203 obtain the graphs. Triplicate study was done to insure the reliability of the methods.

204 **2.2.5 Electrochemical Studies**

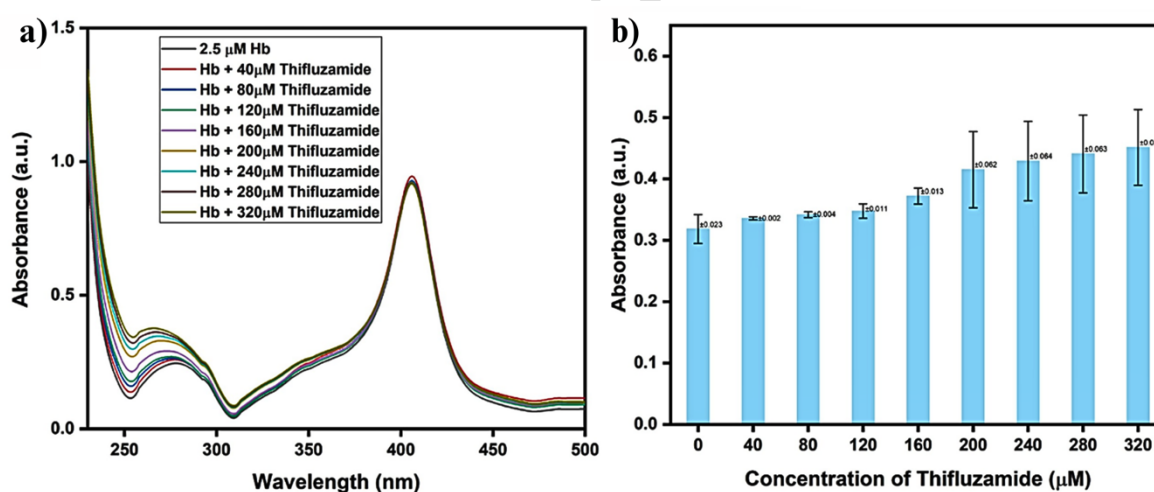
205 An Electrochemical Analyzer (Model 604E) from CHI Inc. was used to conduct
206 electrochemical analysis to study the interaction between TF and Hb. Cyclic voltammograms
207 were conducted within a potential range of -1.8V to 0 V. A series of studies were done with a
208 mixture of 0.1 mM of TF and 10 μM of Hb solution. Three electrode system was used for the
209 measurements with a glassy carbon electrode (GCE) as the working electrode, Ag/AgCl as the
210 reference electrode, and Platinum wire as the counter electrode. Prior to each measurement,
211 GCE was thoroughly cleaned with alumina paste (0.3 microns) and sonicated in deionised
212 water to remove any adsorbed Hb or TF from prior experiments. The solutions were prepared
213 in 1X PBS buffer with pH set to 7.4, and all experiments were conducted at room temperature
214 and triplicate study was also done.

215

216 **3. Results and Discussion**

217 3.1 UV-Visible spectral studies

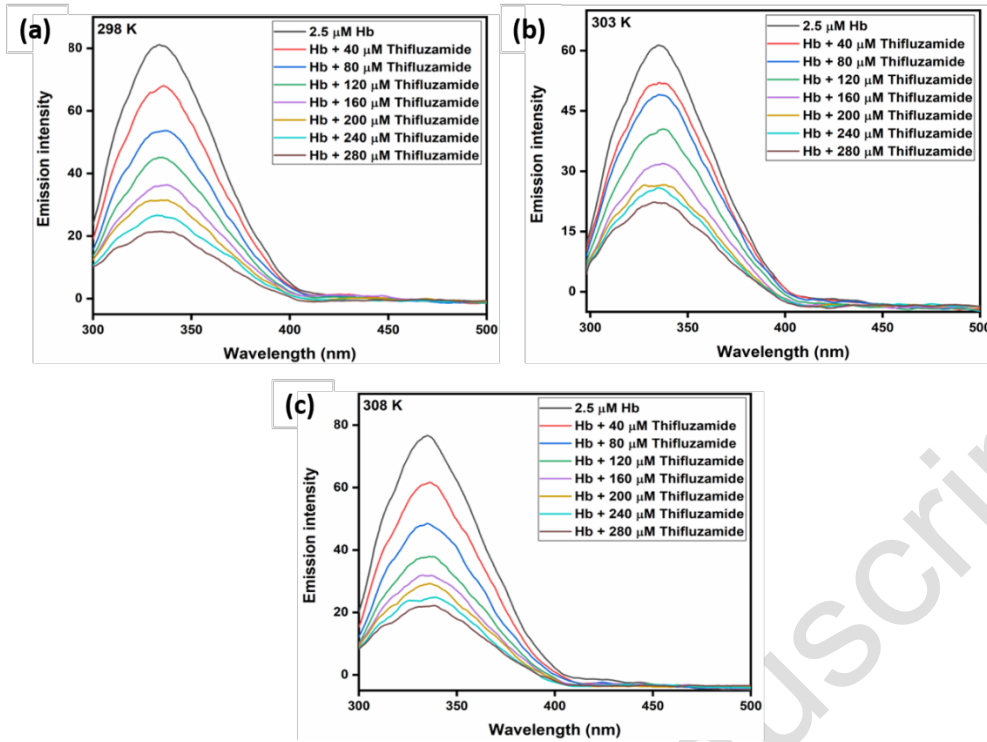
218 Assessing the binding between Hb and TF and conformational rearrangements in the
219 Hb brought on by potential interactions is a common use of UV-visible spectroscopy [16], [36].
220 As in **Figure S1**, Hb showed three peaks at 212, 274 and 406 nm due to n to π^* transitions, π
221 to π^* transitions and the Soret band of porphyrin respectively [37], [38], [39], [40], [41], [42].
222 A significant increase in the intensity of 274 nm peak of Hb was observed on increasing the
223 amount of TF in the solution. This peak corresponds to the aromatic rings of the residues and
224 their environment. The change in intensity and slight red shift corresponds to the change in the
225 electronic environment of the residues indicative of the binding of TF at these hydrophobic
226 positions[43]. A slight increase in the intensity of the Soret band on the addition of TF could
227 correspond to a subtle interaction of TF with the porphyrin ring to potentially alter its electronic
228 environment. The averaged plot of the UV-visible absorption triplicate along with the
229 absorbance graph of Hb in the presence of TF at various concentrations with error bars/standard
230 deviation (**Figure 2a and 2b**), confirms the reproducibility of the UV-visible studies. Higher
231 standard deviations at higher concentrations of TF indicate a destabilised system at higher
232 concentrations of TF.



233 **Figure 2:** UV-visible spectra of Hb solution and mixture containing Hb and TF with varying
234 concentrations of TF at 298 K **a)** averaged plot of Run 1, 2 & 3 and **b)** absorbance graph of Hb
235 at 274 nm against the concentration of TF
236

237 3.2 Fluorescence spectral studies

238 Fluorescence spectroscopy is used to investigate the interaction of TF with Hb. β -Trp37
239 of Hb is the primary cause of Hb's intrinsic fluorescence [44], [45] and the emission band is
240 observed at 336 nm after an excitation at 280 nm. On increasing the amount of TF, a decrease in
241 emission intensity is observed (**Figure 3**).



242
 243 **Figure 3:** Emission spectra of Hb against changing concentrations (0 to 280 μM) of TF at (a)
 244 298 K, (b) 303 K and (c) 308 K

245 The authors recorded the emission spectra at 298 K, 303 K, and 308 K, with a difference of 10
 246 K between the lowest and highest temperatures, to understand the type of quenching (**Figure**
 247 **3**) [46], [47], [48]. When a Hb-TF complex forms in the ground state, static quenching takes
 248 place. While TF-Hb collisional interactions causes dynamic quenching, and F_0/F was found to
 249 have a linear relationship with $[Q]$ for the cases (**Equation 2** is used in the case of dynamic
 250 quenching and for static quenching **Equation 3** is used) [48], [49]. For mixed quenching F_0/F
 251 does not show a linear relation with $[Q]$ (**Equation 4**). Further, all of them have different values
 252 for Stern-Volmer quenching constant, K_{sv} and bimolecular quenching constant, k_q (**Table 1**).

253
$$\frac{F_0}{F} = 1 + K_{sv}[Q] = k_q \tau_0 [Q] \quad (2)$$

254
$$\frac{F_0}{F} = 1 + K_s [Q] \quad (3)$$

255
$$\frac{F_0}{F} = (1 + K_D [Q])(1 + K_S [Q]) \quad (4)$$

256 F_0 and F - fluorescence intensities of Hb without and with TF;

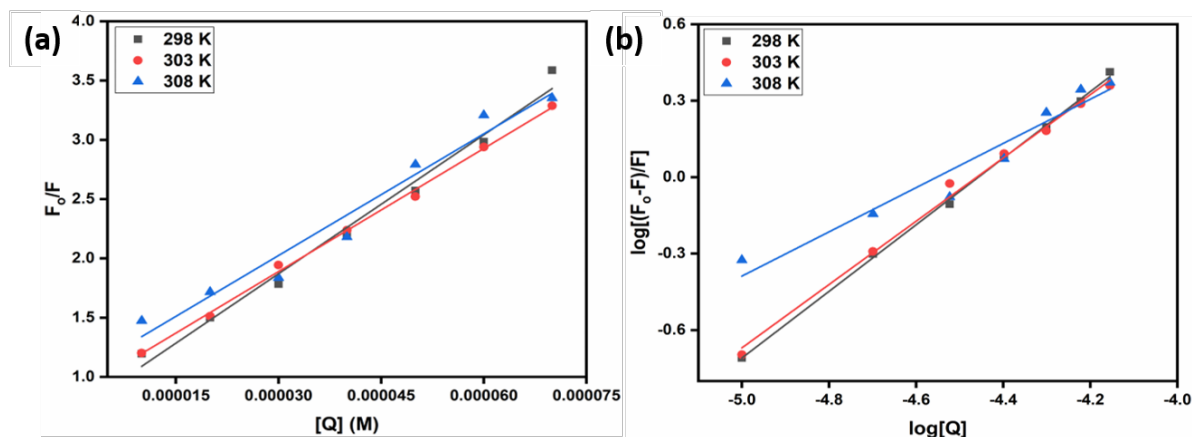
257 K_{sv} - Stern-Volmer quenching constant;

258 k_q - bimolecular quenching constant,

259 $[Q]$ - Concentration of TF:

260 K_S - Static quenching constant or association constant;

261 K_D - Dynamic quenching constant and τ_o ($\sim 10^{-8}$ seconds) [50].
 262 [51], [52], [53], [54] In **Figure 4a**, a linear plot was analyzed using the Stern-Volmer equation
 263 to determine k_q and K_{sv} (**Table 1**). The value of k_q was found to be approximately $10^{12} \text{ M}^{-1}\text{s}^{-1}$,
 264 which exceeded K_{sv} [50–53], indicating static binding [51], [52], [53], [54].



265
 266 **Figure 4:** (a) Stern-Volmer plot (b) Modified Stern-Volmer plot; of Hb against varying
 267 concentrations of TF (0 to 280 μM) at 298, 303, and 308 K

268 **Table 1:** Stern Volmer and bimolecular Quenching constants for TF-Hb binding at 298 K, 303
 269 K and 308 K

Temperature (K)	$K_{sv} (\text{M}^{-1}) \times 10^4$	$k_q (\text{M}^{-1}\text{s}^{-1}) \times 10^{12}$
298	3.90	3.90
303	3.45	3.45
308	3.42	3.42

270
 271 A plot was created using the modified Stern-Volmer equation (**Equation 5**) to determine K_b
 272 and the number of binding sites in the complex (**Figure 4b**) [47]. The equation applied was:

273
$$[47] \log\left(\frac{F_0-F}{F}\right) = \log K_b + n \log[Q] \quad (5)$$

274 In the equation, K_b is the binding constant, and 'n' represents the number of binding sites. At
 275 298 K, the value of K_b is $6.64 \times 10^5 \text{ M}^{-1}$ (**Table 2**) for the TF-Hb complex, and n is nearly equal
 276 to one to indicate the formation of a complex in 1:1 ratio. Different thermodynamic parameters
 277 for TF-Hb have been calculated from van't Hoff's plot (**Figure S2**) drawn using equations 6
 278 and 7.

279
$$\ln K_b = -\frac{\Delta H}{RT} + \frac{\Delta S}{R} \quad (6)$$

280
$$\Delta G = \Delta H - T\Delta S \quad (7)$$

281 R - $8.314 \text{ Jmol}^{-1}\text{K}^{-1}$;

282 ΔG - Gibb's free energy,

283 ΔH - Changes in enthalpy,

284 ΔS - Change in entropy.

285 **Table 2:** Equilibrium dissociation constants and thermodynamic parameters for Hb-TF binding
286 at various temperatures.

Temperature (Kelvin)	K_b (M^{-1})	n	ΔG (kJmol^{-1})	ΔH (kJmol^{-1})	ΔS ($\text{Jmol}^{-1}\text{K}^{-1}$)
298	6.64×10^5	1.36	-34.480	-248.459	-718.05
303	3.46×10^5	1.24			
308	8894.1	0.86			

287

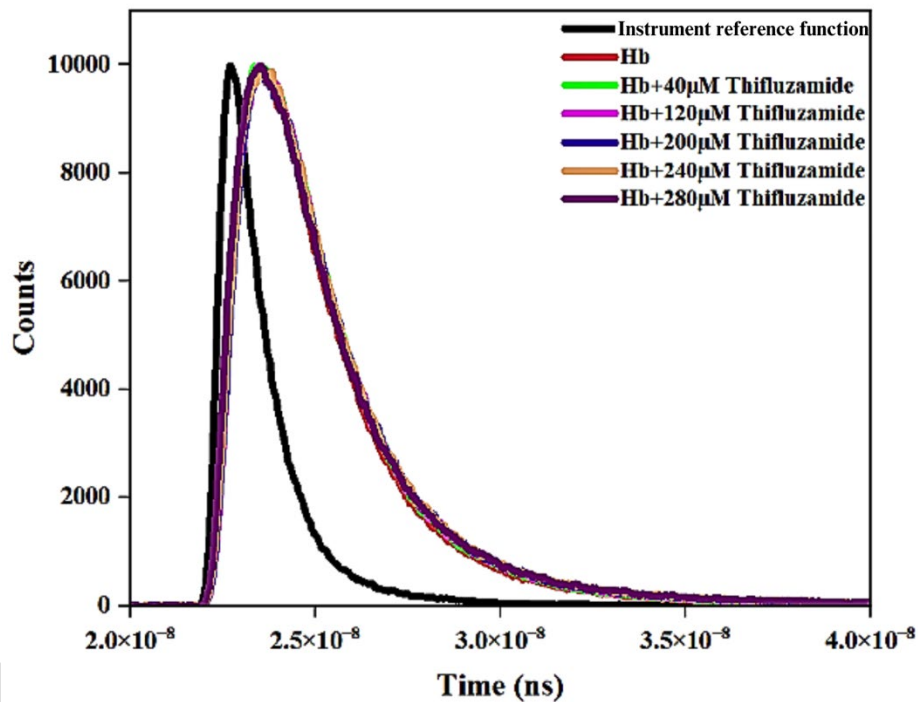
288 The ΔG value is a critical thermodynamic parameter that provides insights into the spontaneity
289 and strength of the binding interaction. The TF-Hb complex was formed due to various
290 interactions like hydrophobic, van der Waals, and hydrogen bonding. From **Table 2**, the value
291 of ΔG was found to be $-34.491 \text{ kJmol}^{-1}$. A negative ΔG value calculated from fluorescence
292 spectroscopy indicates that the binding of TF to Hb is a spontaneous process [55], [56], [57],
293 [58]. Typically, a more negative ΔG value implies stronger binding interactions, such as van
294 der Waals forces, hydrogen bonding, or electrostatic interactions. This thermodynamic analysis
295 is consistent with previously reported data on similar protein-ligand studies [59], [60], [61],
296 [62], thereby validating the robustness of the results.

297

298 3.3 Time-resolved fluorescence spectroscopy

299 The time-resolved fluorescence (TRF) measurements revealed significant insights into the
300 interaction between thifluzamide and Hb. The fluorescence lifetimes (Γ_1 , Γ_2 , Γ_3) and their
301 respective amplitudes (α_1 , α_2 , α_3) were recorded for varying concentrations of thifluzamide (0
302 μM , 40 μM , 120 μM , 200 μM , 240 μM , 280 μM) (**Figure 5**). Hb is a complex protein, and
303 because of its multi-chromophore nature, it exhibits a multi-exponential fluorescence decay.
304 Each fluorescence lifetime reflects different aspects of the dynamics within the protein. The
305 shortest lifetime (Γ_1) typically represents fluorophores on the protein's surface or in highly
306 dynamic regions that relax quickly. The intermediate lifetime (Γ_2) corresponds to moderately
307 exposed fluorophores, and the longest lifetime (Γ_3) is associated with buried or more rigid

308 parts of the protein. A tri-exponential model is essential to capture these varied decay processes
 309 and fully understand the fluorescence properties of Hb. At 0 μM thifluzamide, the fluorescence
 310 lifetimes were $\Gamma_1 = 0.637944$ ns, $\Gamma_2 = 1.59719$ ns, and $\Gamma_3 = 5.1221$ ns, with respective
 311 amplitudes of $\alpha_1 = 16.87\%$, $\alpha_2 = 75.44\%$, and $\alpha_3 = 7.69\%$. The average fluorescence lifetime
 312 (Γ_{av}) was calculated to be 2.350335 ns (**Table 3**). As the concentration of thifluzamide
 313 increased, variations in the fluorescence lifetimes and their amplitudes were observed. For
 314 instance, at 40 μM thifluzamide, the lifetimes were $\Gamma_1 = 0.092472$ ns, $\Gamma_2 = 1.48886$ ns, and Γ_3
 315 = 4.79618 ns, with respective amplitudes of $\alpha_1 = 17.56\%$, $\alpha_2 = 72.51\%$, and $\alpha_3 = 9.92\%$,
 316 resulting in an average lifetime of 2.475685 ns. At the highest concentration of 280 μM , the
 317 lifetimes were $\Gamma_1 = 0.788052$ ns, $\Gamma_2 = 1.72131$ ns, and $\Gamma_3 = 6.06661$ ns, with respective
 318 amplitudes of $\alpha_1 = 20.72\%$, $\alpha_2 = 69.37\%$, and $\alpha_3 = 9.9\%$, and an average lifetime of 2.976385
 319 ns.



320
 321 **Figure 5:** Time-resolved fluorescence (TRF) decay profiles of Hb at different concentrations
 322 of thifluzamide

323
 324 **Table 3:** Fluorescence lifetimes (Γ_1 , Γ_2 , Γ_3) and their respective amplitudes (α_1 , α_2 , α_3) of
 325 hemoglobin (Hb) at varying concentrations of thifluzamide (0 μM , 40 μM , 120 μM , 200 μM ,
 326 240 μM , 280 μM)

Con. (μM)	Γ_1 (ps)	α_1 (%)	Γ_2 (ps)	α_2 (%)	Γ_3 (ps)	α_3 (%)	χ^2	Γ_{av} (ps)
0	0.637	16.87	1.597	75.44	5.122	7.69	1.003	2.350

40	0.092	17.56	1.488	72.51	4.796	9.92	0.956	2.475
120	0.987	31.6	1.767	59.61	5.533	8.79	1.058	2.625
200	0.207	11.31	1.530	77.6	5.215	11.09	1.06	2.704
240	0.146	12.45	1.509	75.31	5.202	12.24	1.15	2.808
280	0.788	20.72	1.721	69.37	6.066	9.9	1.101	2.976

327
328 The observed changes in fluorescence lifetimes with increasing concentrations of thifluzamide
329 suggested interactions between thifluzamide and the Hb molecules, potentially altering the
330 local environment around the fluorophores. These interactions could lead to changes in the
331 conformational dynamics of Hb, affecting its fluorescence properties. The statistical analysis
332 confirmed the significance of these changes, indicating a dose-dependent effect of thifluzamide
333 on the fluorescence lifetimes of Hb (**Figure S3**)[63].

334 As the concentration of thifluzamide increased, we observed shifts in the lifetimes and their
335 corresponding amplitudes, suggesting that thifluzamide interacts with Hb and alters the local
336 environments around the fluorophores. The increase in average lifetime (Γ_{av}) with higher
337 thifluzamide concentrations indicates the occurrence of static quenching, which tends to extend
338 fluorescence lifetimes (Γ_{av}), in contrast to dynamic quenching, which shortens them. This
339 supports our conclusion that static quenching plays a significant role in the Hb-thifluzamide
340 interaction[64].

341

342 **3.4 Circular Dichroism Spectroscopy**

343 The CD spectrum of pure Hb displayed characteristic peaks at 209 nm and 222 nm, indicative
344 of its α -helical structure (**Figure 6**)[65]. Upon the gradual addition of thifluzamide, notable
345 changes were observed in the CD spectra. Specifically, there was a decrease in the ellipticity
346 along with a slight red shift at both the peaks i. e. 209 nm and 222 nm, suggestive of a reduction
347 in the α -helical content of Hb. These spectral changes imply that the binding of thifluzamide
348 induces conformational alterations in helicity of the Hb[66], [67].

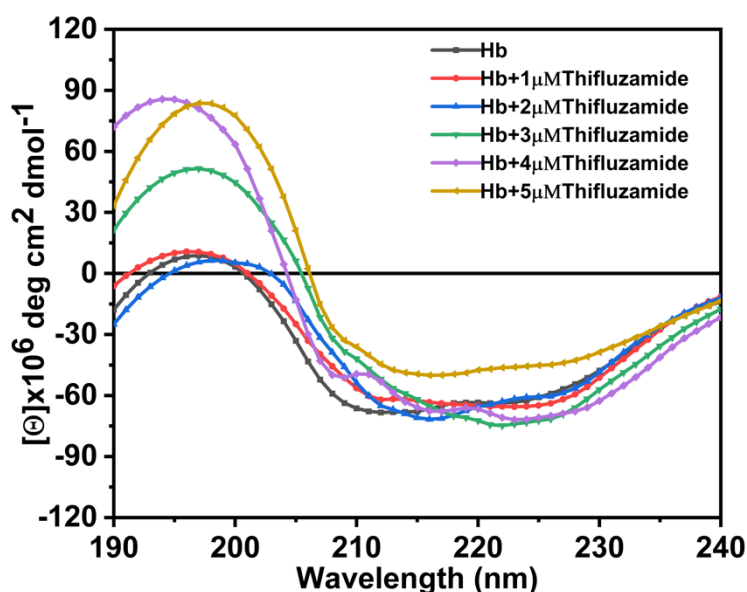
349 The addition of thifluzamide to Hb affects its helical structure. BeStSel webserver was used to
350 determine the secondary of Hb from the data obtained from CD spectroscopy[68], [69]. Native
351 Hb has a helix content of 23.0%, which decreases to 19.3% with 1 μ M thifluzamide, indicating
352 destabilization or helicity disruption. At 2 μ M, the helix content slightly decreased to 16.6%,
353 and drops again with large margin to 8.2% at 3 μ M. The uneven decrease pattern observed in
354 helical content might be due to the dynamic complexation of ligand to protein structure. Once
355 the ligand finds the suitable binding pocket in protein structure it strongly binds to the protein

356 and disrupted structure. So, we suggested that thifluzamide strongly interacted with Hb and
357 disrupts Hb's helical structure (Table 4).

358 **Table 4:** Helix Content of Hb with Varying Concentrations of thifluzamide

S.No.	Sample	Helix (%)
1.	Hb	23.0
2.	Hb + 1 μ M Thifluzamide	19.3
3.	Hb + 2 μ M Thifluzamide	16.6
4.	Hb + 3 μ M Thifluzamide	8.2

359



360

361 **Figure 6:** CD Titration spectra of Hb and Hb-thifluzamide complexes at thifluzamide
362 concentrations (1 μ M-5 μ M).

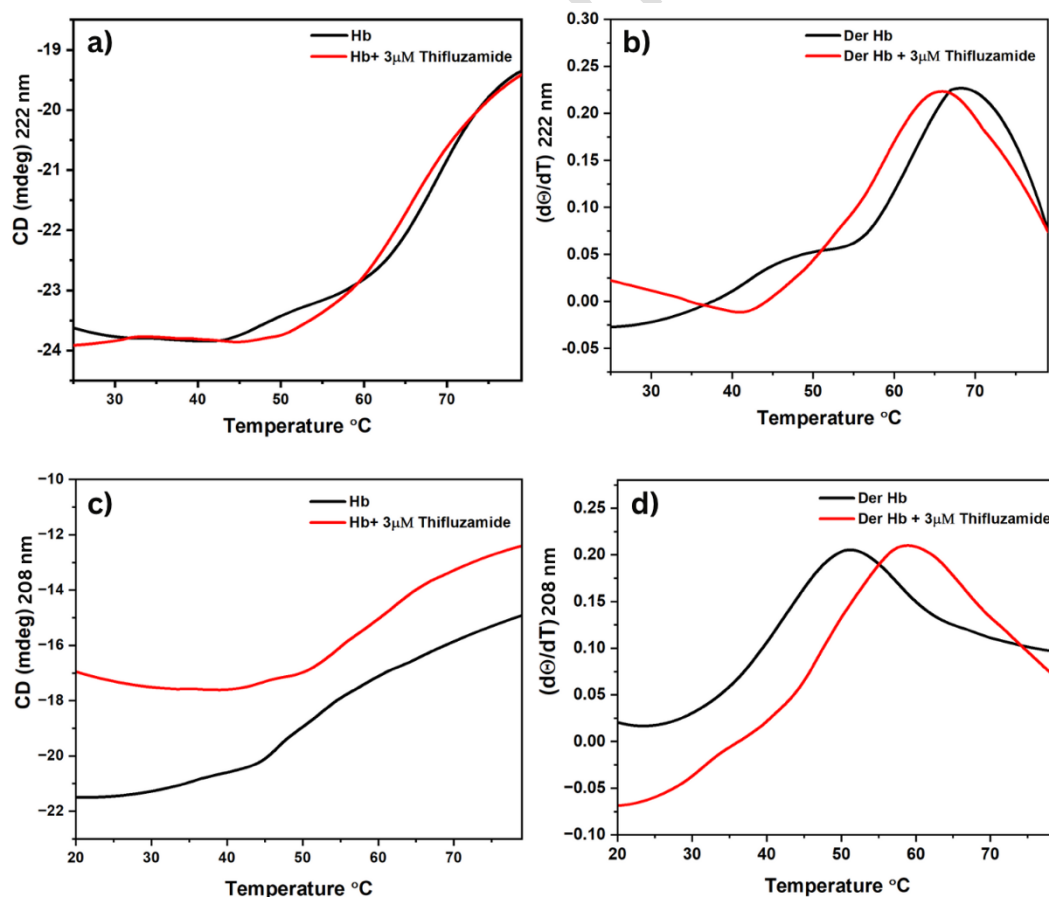
363

364 The observed decrease in α -helicity indicates that thifluzamide binding leads to partial
365 unfolding or reorganization of Hb's secondary structure. This interaction likely to cause the
366 protein to adopt a less ordered conformation. The structural changes observed in the CD spectra
367 suggest that thifluzamide interacts with Hb, causing significant alterations in its secondary
368 structure. These conformational changes could have important biological implications,
369 potentially affecting the functional properties of Hb, such as its oxygen-binding capacity and
370 stability. Further studies, including fluorescence spectroscopy and molecular docking, could
371 provide deeper insights into the binding mechanism and structural effects of thifluzamide on
372 Hb.

373

374 3.5 Thermal melt circular dichroism

375 The CD melting spectroscopy analysis of hemoglobin (Hb) with thifluzamide revealed
376 significant differences in thermal stability at different wavelengths, providing insights into how
377 thifluzamide binding affected Hb's structure. **Figure 7** contains the CD melting profiles of Hb
378 and Hb with thifluzamide at 222 nm and 208 nm. At 222 nm, which is sensitive to the α -helix
379 content, the melting temperature T_m for Hb was 68.2°C, while for Hb-thifluzamide, it was
380 65.1°C. This lower T_m for Hb-thifluzamide indicated that thifluzamide destabilized the α -
381 helical regions, making them less stable and more prone to unfolding at lower temperatures.
382 Conversely, at 208 nm, which reflected the overall secondary structure including both α -helices
383 and β -sheets, the T_m for Hb was 51.15°C, whereas for Hb-thifluzamide, it was 58.74°C. This
384 suggested that thifluzamide altered the native structure of Hb, potentially disrupting the
385 hydrogen bonding or hydrophobic interactions critical for maintaining its tertiary or quaternary
386 structure [70]. These interactions highlighted the impact of thifluzamide on the structural
387 stability of Hb, providing insights into the binding of thifluzamide with Hb. The thermal melt
388 circular dichroism results were in good agreement with the CD titration studies, which also
389 revealed gradual binding of thifluzamide to Hb resulting in native structural changes in Hb
390 [71], [72].



392 **Figure 7:** a) CD Melting profiles at 222 nm of Hb and Hb with 3 μ M thifluzamide (b), first
393 derivative plot of the melting profiles (222 nm), c) CD melting profiles at 208 nm of Hb and
394 Hb with 3 μ M thifluzamide, and d) first derivative plot of the melting profiles (208 nm).
395 [70][71], [72]

396 **3.6 *In silico* studies**

397 **3.6.1 Molecular docking**

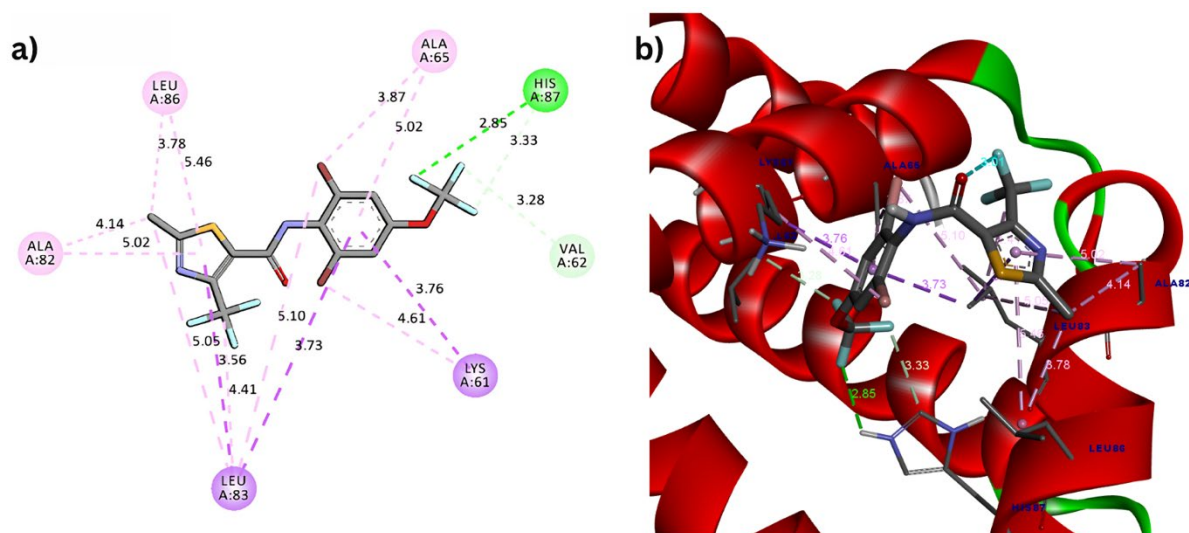
398 Interactions between TF and Hb were analysed using molecular docking. The nature of forces
399 in the formation of the TF-Hb complex were hydrophobic, van der Waals, hydrogen bonding
400 and electrostatic interactions. The binding energy for the TF-Hb complex was found to be -6.1.
401 Notably, it demonstrated effective interactions with ALA (65, 82), HIS (87), VAL (62), LYS
402 (61) and LEU (83, 86).

403 Various interactions were observed, including hydrogen bonding and hydrophobic interactions
404 (π -alkyl, π -sigma and π - π stacked). HIS:87 and VAL:62 formed hydrogen bonds with -CF₃
405 moiety. LYS:61 interacted with the phenyl ring and the attached Bromine. LEU:83 showed a
406 maximum number of interactions (five) with the phenyl ring, bromine attached to the phenyl
407 ring, thiazole group and substituent of thiazole (-CH₃ and -CF₃). ALA:82 and LEU (86 & 83)
408 showed interactions with the thiazole moiety, as shown in **Figure 8**.

409 The binding site of TF in Hb (PDB ID: 2DN1) was a well-defined pocket characterized by a
410 combination of polar and nonpolar residues. Key interactions were observed with His A:87,
411 which likely formed hydrogen bonds with TF, providing specificity and stabilization. The
412 presence of Val A:62 contributed to the hydrophobic nature of the pocket, facilitating nonpolar
413 interactions that further stabilized the ligand. Additionally, Lys A:61 may have participated in
414 electrostatic interactions due to its positively charged side chain, enhancing binding affinity.
415 The pocket also included small, nonpolar residues like Ala A:65 and Ala A:82, alongside larger
416 hydrophobic residues such as Leu A:83 and Leu A:86. These residues contributed to the
417 hydrophobic environment, conducive to stabilizing TF's hydrophobic moieties. The spatial
418 arrangement and combination of these residues created a versatile binding pocket capable of
419 accommodating various functional groups of TF through a blend of hydrophobic, electrostatic,
420 and hydrogen bonding interactions.

421

422



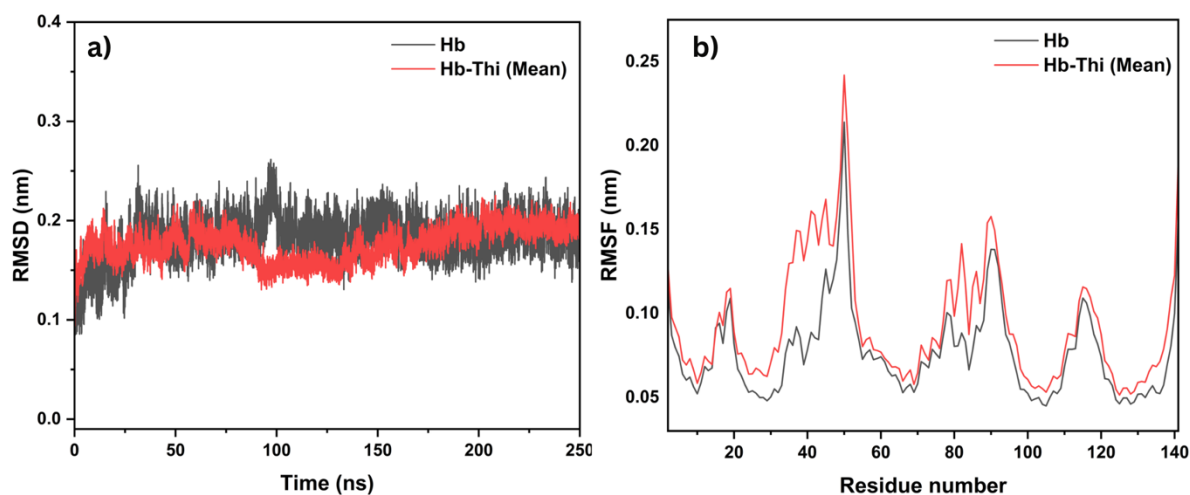
423

424 **Figure 8: a)** Two-dimensional and **b)** three-dimensional views of interactions between TF and
 425 Hb (2DN1) in Run1. Two-dimensional docked pose of TF in **c)** Run 2 and **d)** Run 3

426 3.6.2 Molecular Dynamics Simulations

427 *RMSD and RMSF*

428 MD Simulations of Hb with and without TF was performed for 250 ns using GROMACS three
 429 times. TIP3P model was employed with a temperature of 298 K using cubic box type.
 430 Trajectories obtained after simulations were first centred with periodic boundary condition
 431 'pbc', which keeps the centre of mass of the protein in the simulation box. Obtained trajectories
 432 were plotted to understand the stability of the Hb with and without TF. **Figure 9a** represents
 433 the root mean square deviation (RMSD) plot for the Hb and Hb-TF (mean). The RMSD value
 434 of Hb alone stabilised initially, with no significant changes observed. However, in the case of
 435 the Hb-TF complex, decrease in RMSD after 90 ns was observed indicating stabilisation of the
 436 complex [73], [74], [75]. The fluctuations in the RMSD values remained in the acceptable
 437 range, implying a stable system. **Figure 9b** illustrates the root mean square fluctuations
 438 (RMSF) of residues of Hb in the absence and presence of TF during MD simulations conducted
 439 for 250 ns. It measures the average deviation of residues from their mean position. Lower
 440 RMSF values indicate rigidity of the protein structure, while higher values suggests
 441 flexibility[76]. In the case of the Hb-TF complex increased average fluctuations were observed
 442 throughout the simulation. Increased fluctuations in the Hb-TF complex suggest changes in the
 443 structure of the Hb protein. RMSD and RMSF analysis suggest binding of TF molecule with
 444 Hb, resulting in a change in the protein structure.



445

446 **Figure 9. a)** Root mean square deviation and, **b)** root means square fluctuations of Hb and Hb-
 447 TF complex for 250ns

448 MD simulation of the Hb-TF complex was done three times to increase the reliability of the
 449 study. All the parameters and conditions were kept identical. **Figure S4a** contains RMSD
 450 obtained from the trajectories of Run 1, 2, and 3. Average RMSD values for Run 1, 2 and 3
 451 were 0.170, 0.181 and 0.176 Å, respectively[77]. The standard deviation for these values was
 452 found to be 0.0055 Å and relative standard deviation (RSD) of 3.14 %, which is in an
 453 acceptable range[78], [79]. Similar patterns in the variation of RMSD were observed in Runs
 454 1, 2, and 3 during the simulation, i.e., a gradual decrease in RMSD after 100 ns followed by
 455 equilibration. **Figure S4b** contains the RMSF of triplicate MD simulations of the Hb-TF
 456 complex for 250 ns. A similar fingerprint pattern in the RMSF was observed in Run 1, 2 and 3
 457 indicating the reproducibility of the MD simulations.

458 *Number of Hydrogen Bonds*

459 The number of hydrogen bonds between the ligand and the protein were estimated from the
 460 trajectory of Run 1, Run 2 and Run 3 and plotted in **Figure S5**. The observed fluctuation in the
 461 number of hydrogen bonds between the Hb protein and TF during the initial phase of the
 462 simulation (1-3 bonds) suggests a dynamic interaction. However, after 120ns, the number of
 463 hydrogen bonds stabilised at one, indicating that the TF molecule reached equilibrium within
 464 the protein's active site, resulting in a constant interaction pattern thereafter and stable complex
 465 formation[80], [81]. Similar results were obtained in Run 2 and 3, with one stable hydrogen
 466 bond and a few variations with increased hydrogen bonds to two and three for a short period.

467 *Secondary structure analysis*

468 The secondary structure of Hb was analyzed using the STRIDE web server and MD simulation
 469 trajectories[82]. The structure of Hb was extracted at regular intervals (0 ns, 50 ns, 100 ns, 150

470 ns, 200 ns, and 250 ns) from the MD simulation of the Hb-thifluzamide complex. **Figure S6**
471 illustrates the secondary contributions of each residue in the protein at these intervals, as
472 obtained from the STRIDE web server. Manual calculations revealed that the percentage of
473 alpha helix in the structure varied between 72 % and 80 % during the simulations. This
474 indicates that the binding of thifluzamide induced changes in the native secondary structure of
475 Hb, potentially altering its normal function.

476

477 3.7 Electrochemical Analysis

478 Electrochemical analysis was done using cyclic voltammetry and tafel plot analysis.
479 Voltammograms of ten consecutive scans of 0.1 mM solution of TF were recorded between -
480 1.8 V to 0 V (**Figure 10a**). A single reductive peak was observed around -1.4 V, corresponding
481 to the irreversible reduction of TF at the electrode surface. A broad and small peak at -0.6 V
482 was due to the solvent used. It was observed that the peak current reduced with the number of
483 scans, possibly due to the deposition of reduced TF molecules onto the electrode surface,
484 blocking the sites for new molecules[83]. Thus, the GCE was washed before every scan in
485 further studies.

486 Scan rate study of 0.1 mM solution of TF was done at 200mV/s, 300mV/s, 400mV/s, 500mV/s
487 and 600mV/s scan rates. It is important to characterise the electrochemical process occurring
488 on the electrode surface as it will help to understand the changes that occurred with the addition
489 of Hb. **Figure 10c** illustrates the cyclic voltammograms of TF with various scan rates, from
490 200 to 600 mV/s. On increasing scan rate, the cathodic peak current becomes more negative.
491 To quantify this relationship, the cathodic peak current was plotted against the square root of
492 the scan rate. The relationship between peak current and scan rate for an irreversible reaction
493 can be described by the modified Randles-Sevcik equation[84], [85]:

$$494 \quad I_p = (2.99 \times 10^5)n\alpha^{1/2}AD^{1/2}Cv^{1/2}$$

495 where:

496 α – transfer coefficient,

497 I_p - cathodic peak current (A),

498 n -number of electrons involved in the redox process,

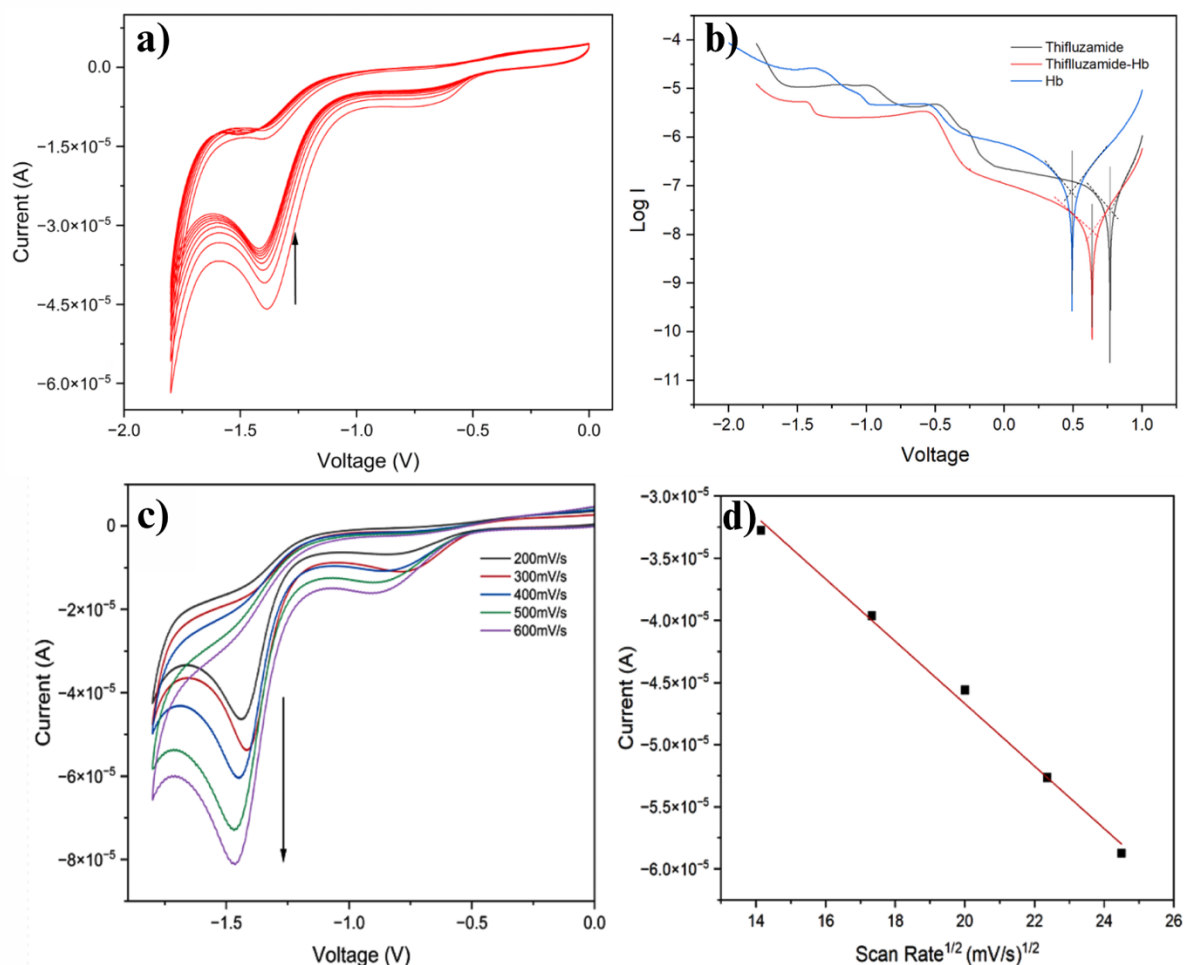
499 A - electrode area (cm²),

500 D - diffusion coefficient (cm²/s),

501 C - concentration of the analyte (mol/cm³),

502 v - scan rate (V/s).

503 The linear increase in peak current upon increasing the scan rate was observed, inferring that
504 the reduction of TF at the electrode surface is a diffusion-controlled process.



505

506

507 **Figure 10.** a) Multi-scan cyclic voltammograms of 0.1mM solution of TF, b) Tafel plot of TF,
508 Hb and the mixture of TF-Hb at 30 minutes of stirring, c) cyclic voltammograms of 0.1mM
509 solution of TF at 200mV/s, 300mV/s, 400mV/s, 500mV/s and 600mV/s scan rate and d)
510 cathodic peak current versus scan rates (200-600 mV/s).

511 Tafel plot of the pesticide solution and the mixture of pesticide and Hb solution (after 30 min
512 of stirring) was recorded between the potential range of -1.8 V and 1 V at 10 mV/s scan with
513 1×10^{-5} sensitivity (Figure 10b). The cathodic and anodic slopes for pesticide solution were
514 found to be 3.37 and 5.96 respectively. Thus, the rate of cathodic processes occurring at the
515 electrode surface was higher than anodic reactions, owing to the lower Tafel slope[86]. Similar
516 results were observed for the mixture of Hb and TF with cathodic and anodic slope of 2.52 and

517 4.08 (**Table 5**). This confirms the irreversibility of TF reduction. The rate of anodic reactions
518 occurring at the electrode surface was much slower in the case of pure TF solution

519 **Table 5.** Cathodic and anodic slopes of Hb, TF and Hb-TF (30 min) obtained from tafel
520 plot analysis

S.No.	System	Cathodic slope	Anodic slope
1.	Hb	3.03	3.47
2.	Thifluzamide	3.37	5.96
3.	Hb-thifluzamide	2.52	4.08

521
522 A time-dependent study of the mixture of TF and Hb solution was done. Cyclic voltammograms
523 were recorded at regular intervals as shown in **Figure S7a**. It was observed that the
524 characteristic reductive peak of TF reduced gradually with time in the presence of Hb.
525 Indicating gradual binding of the pesticide with the Hb protein. It was observed that in the
526 presence of Hb the peak current of TF reduced significantly in the first 15 minutes. Peak
527 reduction can be attributed to the unavailability of TF molecules at the electrode surface, which
528 might be due to the binding of TF with Hb, the possibility of Hb blocking the electrode surface
529 was eliminated by cleaning the electrodes prior to each reading. At 60 minutes, the peak
530 disappeared completely. The pesticide concentration was reduced gradually to the limit of
531 detection.

532 Triplicate of the time dependent study of TF-Hb binding was performed. **Figure S7** contains
533 the cyclic voltammograms of Run 1, 2 and 3 along with the mean of current response at the
534 reductive potential of TF at various time periods. In **Figure S7d**, it was observed that the
535 standard deviation in the current response reduced gradually and stabilised after 30 min to a
536 minimal value ($\sim \pm 0.6\mu\text{A}$). A high standard deviation in initial measurements indicates initial
537 variability in the system, followed by a low standard deviation indicating equilibration of the
538 system over time. The reproducibility and reliability of the experiment were confirmed with
539 the low standard deviation in the peak current after 30 min.

540

541

542 **4. Conclusion**

543 The study utilised a multidisciplinary approach, incorporating spectroscopic, electrochemical,
544 and computational methods, to investigate the interaction between TF and Hb. Our
545 spectroscopic analyses, including UV-visible and fluorescence spectroscopy, confirmed the

546 formation of a stable TF-Hb complex. The observed decrease in the Stern-Volmer quenching
547 constant with rising temperature indicated static quenching, supported by a bimolecular
548 quenching constant of $3.90 \times 10^{12} \text{ M}^{-1} \text{ s}^{-1}$ (298 K), pointing to static quenching involvement in
549 TF-Hb binding. At 298 K, the binding constant was determined to be $6.64 \times 10^5 \text{ M}^{-1}$, with a 1:1
550 binding ratio. The free energy change (ΔG) of $-34.491 \text{ kJ mol}^{-1}$ further corroborated the
551 stability of the TF-Hb complex. Increase in 274 nm peak confirmed binding of TF with
552 aromatic regions of Hb. CD studies confirmed that thifluzamide binds with Hb, reducing its
553 helix structure. The decrease in melting temperature T_m from $68.2 \text{ }^\circ\text{C}$ to $65.1 \text{ }^\circ\text{C}$ (222 nm)
554 further indicated Hb destabilization upon thifluzamide introduction. Molecular docking studies
555 highlighted specific interactions between TF and key amino acid residues of Hb, including
556 ALA, HIS, VAL, LYS and LEU, with a binding energy of $-25.52 \text{ kJ mol}^{-1}$. Molecular dynamics
557 simulations provided additional validation, showing conformational changes and stable
558 complex formation through RMSD and RMSF analysis. Electrochemical studies offered
559 further evidence of interaction, a consistent reduction in the TF reduction peak in the presence
560 of Hb over time. Overall, our findings confirm the formation of a stable complex between TF
561 and Hb. These insights reveal that TF binding induces structural changes in Hb, which might
562 hamper its normal function, highlighting the potential impact of TF on the biological activity
563 of Hb and broader implications for biological systems.

564

565

566

567

568

569

570

571

572

573

574

575 **Declarations**

576 **Ethical Approval** Not Applicable

577 **Competing interests** There is also no potential conflict of interest in any way.

578 **Authors' contributions**

579 **Sandeep Yadav, Shubham Sewariya, Anirudh Pratap Singh Raman, Arun, Pallavi Jain,**
580 **Anju Singh** – Performed calculations, analysis and draft writing

581 **Ramesh Chandra, Prashant Singh** - Supervision, finalization of the manuscript

582 **Kamlesh Kumari** – Conceptualisation, and finalisation of the manuscript

583 **Funding** Dr Kamlesh Kumari conveys thanks to IoE, University of Delhi for the financial
584 support. (IoE/2023-24/12/FRP)

585 **Availability of data and materials** Data will be made available on request of reader.

586 **Acknowledgement** Authors are thankful to Professor B. Jayaram for utilising the facilities of
587 SCFBio, Indian Institute of Technology, Delhi, India. Authors convey thanks to Dr. Kawar Lal
588 Dabodhia, GSP Crop Science Pvt Ltd, Navrangpura, Ahmedabad, Gujarat, India. for providing
589 thifluzamide for carrying out the experiment experiments. Authors would like to acknowledge
590 USIC, University of Delhi, Delhi, India, for providing facilities of circular dichroism
591 experiments. Authors would also like to acknowledge Prof. Rajan Patel, Centre for
592 Interdisciplinary Research in Basic Sciences, Jamia Millia Islamia, Delhi, India for providing
593 facilities for time-resolved fluorescence spectroscopy.

594

595 **References**

596

597 [1] R. Kaur *et al.*, "Pesticides: An alarming detrimental to health and environment,"
598 *Science of The Total Environment*, vol. 915, p. 170113, Mar. 2024, doi:
599 10.1016/J.SCITOTENV.2024.170113.

600 [2] S. Mostafalou and M. Abdollahi, "The susceptibility of humans to neurodegenerative
601 and neurodevelopmental toxicities caused by organophosphorus pesticides," *Arch*
602 *Toxicol*, vol. 97, no. 12, pp. 3037–3060, Oct. 2023, doi: 10.1007/S00204-023-03604-2.

603 [3] I. de A. A. Fernandes *et al.*, "The bitter side of teas: Pesticide residues and their
604 impact on human health," *Food and Chemical Toxicology*, vol. 179, p. 113955, Sep.
605 2023, doi: 10.1016/J.FCT.2023.113955.

606 [4] W. Chen, M. Li, W. Li, X. Wu, and L. Han, "Dissipation and Residue Level of
607 Thifluzamide in Rice Field Ecosystem," *J Chem*, vol. 2015, no. 1, p. 848252, Jan. 2015,
608 doi: 10.1155/2015/848252.

609 [5] P. Maienfisch and A. J. F. Edmunds, "Thiazole and Isothiazole Ring-Containing
610 Compounds in Crop Protection," in *Advances in Heterocyclic Chemistry*, vol. 121,
611 Academic Press, 2017, pp. 35–88. doi: 10.1016/BS.AIHCH.2016.04.010.

612 [6] R. Oldenkamp *et al.*, "Incorporating climate projections in the environmental risk
613 assessment of pesticides in aquatic ecosystems," *Integr Environ Assess Manag*, vol.
614 20, no. 2, pp. 384–400, Mar. 2024, doi: 10.1002/IEAM.4849.

615 [7] Pawan Kumar *et al.*, "Impact of Pesticides Application on Aquatic Ecosystem and
616 Biodiversity: A Review," *Biology Bulletin*, vol. 50, no. 6, pp. 1362–1375, Dec. 2023, doi:
617 10.1134/S1062359023601386/TABLES/4.

- 618 [8] M. Kim *et al.*, "Monitoring and Risk Assessment of Pesticide Residues in Fishery
619 Products Using GC–MS/MS in South Korea," *Toxics*, vol. 12, no. 4, p. 299, Apr. 2024,
620 doi: 10.3390/TOXICS12040299.
- 621 [9] K. Li *et al.*, "Computation-Directed Molecular Design, Synthesis, and Fungicidal
622 Activity of Succinate Dehydrogenase Inhibitors," *J Agric Food Chem*, vol. 71, no. 49,
623 pp. 19372–19384, Dec. 2023, doi:
624 10.1021/ACS.JAFC.3C05232/ASSET/IMAGES/LARGE/JF3C05232_0007.JPEG.
- 625 [10] Y. Yang, J. Chang, D. Wang, H. Ma, Y. Li, and Y. Zheng, "Thifluzamide exposure induced
626 neuro-endocrine disrupting effects in zebrafish (*Danio rerio*)," *Arch Toxicol*, vol. 95, no.
627 12, pp. 3777–3786, Dec. 2021, doi: 10.1007/S00204-021-03158-1/FIGURES/7.
- 628 [11] Z. Yan *et al.*, "Thiazolamide derivatives containing diphenyl ethers moiety: design,
629 synthesis, fungicidal activity and docking study," *Journal of Chemical Sciences*, vol.
630 135, no. 3, 2023, doi: 10.1007/s12039-023-02184-z.
- 631 [12] L. Chen, Z. Yang, and H. Liu, "Hemoglobin-Based Oxygen Carriers: Where Are We Now
632 in 2023?," *Medicina (B Aires)*, vol. 59, no. 2, p. 396, Feb. 2023, doi:
633 10.3390/MEDICINA59020396.
- 634 [13] F. Spyraakis, F. J. Luque, and C. Viappiani, "Structural analysis in nonsymbiotic
635 hemoglobins: What can we learn from inner cavities?," 2011. doi:
636 10.1016/j.plantsci.2011.03.021.
- 637 [14] C. Savino *et al.*, "Pattern of cavities in globins: The case of human hemoglobin,"
638 *Biopolymers - Peptide Science Section*, vol. 91, no. 12, 2009, doi: 10.1002/bip.21201.
- 639 [15] S. Yadav, S. Sewariya, P. Singh, R. Chandra, P. Jain, and K. Kumari, "Analytic and In Silico
640 Methods to Understand the Interactions between Dinotefuran and Haemoglobin,"
641 *Chem Biodivers*, p. e202400495, 2024, doi: 10.1002/cbdv.202400495.
- 642 [16] S. Yadav *et al.*, "Employing Spectroscopic, Electrochemical, and In Silico Research to
643 Investigate the Interaction of Ofloxacin, Antibacterial Drug With the Haemoglobin,"
644 *ChemistrySelect*, vol. 9, p. e20240077, 2024, doi: 10.1002/slct.202400770.
- 645 [17] F. Ding, B. Y. Han, W. Liu, L. Zhang, and Y. Sun, "Interaction of imidacloprid with
646 hemoglobin by fluorescence and circular dichroism," *J Fluoresc*, vol. 20, no. 3, pp.
647 753–762, May 2010, doi: 10.1007/S10895-010-0618-0/FIGURES/11.
- 648 [18] A. Doroudian, M. Emadi, R. Hosseinzadeh, and P. Maghami, "Biological and Molecular
649 Effects of Pesticides on Human Health," in *Pesticides - Updates on Toxicity, Efficacy and
650 Risk Assessment*, IntechOpen, 2022. doi: 10.5772/INTECHOPEN.104811.
- 651 [19] N. Mhadhbi *et al.*, "Physico-Chemical Properties, Pharmacokinetics, Molecular
652 Docking and In-Vitro Pharmacological Study of a Cobalt (II) Complex Based on 2-
653 Aminopyridine," *ChemistrySelect*, vol. 7, no. 3, p. e202103592, Jan. 2022, doi:
654 10.1002/SLCT.202103592.
- 655 [20] S. Gatfaoui, N. Issaoui, T. Roisnel, and H. Marouani, "Synthesis, experimental and
656 computational study of a non-centrosymmetric material 3-methylbenzylammonium
657 trioxonitrate," *J Mol Struct*, vol. 1225, p. 129132, Feb. 2021, doi:
658 10.1016/J.MOLSTRUC.2020.129132.
- 659 [21] M. Medimagh *et al.*, "DFT and molecular docking study of the effect of a green
660 solvent (water and DMSO) on the structure, MEP, and FMOs of the 1-ethylpiperazine-
661 1,4-dium bis(hydrogenoxalate) compound," *J Mol Liq*, vol. 369, p. 120851, Jan. 2023,
662 doi: 10.1016/J.MOLLIQ.2022.120851.
- 663 [22] F. Hammami, N. Issaoui, and S. Nasr, "Investigation of hydrogen bonded structure of
664 urea-water mixtures through Infra-red spectroscopy and non-covalent interaction

665 (NCI) theoretical approach," *Comput Theor Chem*, vol. 1199, p. 113218, May 2021,
666 doi: 10.1016/J.COMPTC.2021.113218.

667 [23] Alka, V. K. Vishvakarma, S. Yadav, P. Singh, and P. Jain, "In Vitro, In Silico, ADME and
668 Theoretical Analysis of Mn(II) and Co(II) Complexes Derived from Methyl-(Z)-N'-
669 Carbamothioylcarbamohydrazonate Schiff Base Ligand," *Chem Biodivers*, vol. 20, no.
670 6, p. e202300042, Jun. 2023, doi: 10.1002/CBDV.202300042.

671 [24] A. Kumar *et al.*, "Synthesis, antimicrobial, antibiofilm and computational studies of
672 isatin-semicarbazone tethered 1,2,3-triazoles," *Bioorg Chem*, vol. 133, p. 106388, Apr.
673 2023, doi: 10.1016/J.BIOORG.2023.106388.

674 [25] G. M. Morris *et al.*, "AutoDock4 and AutoDockTools4: Automated Docking with
675 Selective Receptor Flexibility," *J Comput Chem*, vol. 30, no. 16, p. 2785, Dec. 2009, doi:
676 10.1002/JCC.21256.

677 [26] D. Romani, O. Noureddine, N. Issaoui, and S. A. Brandán, "Properties and reactivities
678 of niclosamide in different media, a potential antiviral to treatment of COVID-19 by
679 using DFT calculations and molecular docking," *Biointerface Res Appl Chem*, vol. 10,
680 no. 6, 2020, doi: 10.33263/BRIAC106.72957328.

681 [27] J. Saraswat, A. Firoz, M. R. Kamli, and R. Patel, "Improved Antibacterial Activity of
682 Peptide Nisin with Pyrrole-Based Ionic Liquids Having
683 Bis(trifluoromethylsulfonyl)imide as a Counterion: A Synergistic Approach to Combat
684 Bacterial Infections," *ACS Omega*, vol. 9, no. 2, 2024, doi: 10.1021/acsomega.3c07824.

685 [28] D. Kumar *et al.*, "A review targeting the infection by CHIKV using computational and
686 experimental approaches," *J Biomol Struct Dyn*, vol. 40, no. 17, pp. 8127–8141, Nov.
687 2022, doi: 10.1080/07391102.2021.1904004.

688 [29] X.-Y. Meng, H.-X. Zhang, M. Mezei, and M. Cui, "Molecular docking: a powerful
689 approach for structure-based drug discovery," *Curr Comput Aided Drug Des*, vol. 7,
690 no. 2, pp. 146–157, Jun. 2011, doi: 10.2174/157340911795677602.

691 [30] T. Makarewicz and R. Kaźmierkiewicz, "Molecular dynamics simulation by GROMACS
692 using GUI plugin for PyMOL," *J Chem Inf Model*, vol. 53, no. 5, pp. 1229–1234, May
693 2013, doi: 10.1021/CI400071X/ASSET/IMAGES/MEDIUM/CI-2013-00071X_0007.GIF.

694 [31] H. BEKKER *et al.*, "GROMACS - A PARALLEL COMPUTER FOR MOLECULAR-DYNAMICS
695 SIMULATIONS," *PHYSICS COMPUTING '92*, pp. 252–256, 1993, doi:
696 10.2/JQUERY.MIN.JS.

697 [32] M. J. Abraham *et al.*, "GROMACS: High performance molecular simulations through
698 multi-level parallelism from laptops to supercomputers," *SoftwareX*, vol. 1–2, pp. 19–
699 25, Sep. 2015, doi: 10.1016/J.SOFTX.2015.06.001.

700 [33] P. Bjelkmar, P. Larsson, M. A. Cuendet, B. Hess, and E. Lindahl, "Implementation of the
701 CHARMM Force Field in GROMACS: Analysis of Protein Stability Effects from
702 Correction Maps, Virtual Interaction Sites, and Water Models," *J Chem Theory
703 Comput*, vol. 6, no. 2, pp. 459–466, Jan. 2010, doi: 10.1021/ct900549r.

704 [34] A. P. S. Raman, J. Tomar, P. Jain, A. Kumar, P. Singh, and K. Kumari, "Exploring the
705 Molecular Interactions between Acyclovir and Hormones: Insights from Density
706 Functional Theory Calculations," *ChemistrySelect*, vol. 8, no. 40, p. e202303320, Oct.
707 2023, doi: 10.1002/SLCT.202303320.

708 [35] A. Kumar, K. Kumari, A. P. S. Raman, P. Jain, D. Kumar, and P. Singh, "An insight for the
709 interaction of drugs (acyclovir/ganciclovir) with various ionic liquids: DFT calculations
710 and molecular docking," *J Phys Org Chem*, vol. 35, no. 1, p. e4287, Jan. 2022, doi:
711 10.1002/POC.4287.

- 712 [36] W. L. Nichols, B. H. Zimm, and L. F. Ten Eyck, "Conformation-invariant structures of the
713 $\alpha 1\beta 1$ human hemoglobin dimer," *J Mol Biol*, vol. 270, no. 4, pp. 598–615, Jul. 1997,
714 doi: 10.1006/JMBI.1997.1087.
- 715 [37] J. H. Shi, Y. Y. Lou, K. L. Zhou, and D. Q. Pan, "Elucidation of intermolecular interaction
716 of bovine serum albumin with Fenhexamid: A biophysical prospect," *J Photochem
717 Photobiol B*, vol. 180, pp. 125–133, Mar. 2018, doi: 10.1016/j.jphotobiol.2018.01.025.
- 718 [38] Q. Wang *et al.*, "Binding interaction of atorvastatin with bovine serum albumin:
719 Spectroscopic methods and molecular docking," *Spectrochim Acta A Mol Biomol
720 Spectrosc*, vol. 156, pp. 155–163, Mar. 2016, doi: 10.1016/j.saa.2015.12.003.
- 721 [39] J. H. Shi, Q. Wang, D. Q. Pan, T. T. Liu, and M. Jiang, "Characterization of interactions of
722 simvastatin, pravastatin, fluvastatin, and pitavastatin with bovine serum albumin:
723 multiple spectroscopic and molecular docking," *J Biomol Struct Dyn*, vol. 35, no. 7, pp.
724 1529–1546, May 2017, doi: 10.1080/07391102.2016.1188416.
- 725 [40] N. Kritika, M. Pant, M. Yadav, A. K. Verma, A. K. Mahapatro, and I. Roy, "Comparative
726 analysis of cobalt ferrite and iron oxide nanoparticles using bimodal hyperthermia,
727 along with physical and in silico interaction with human hemoglobin," *J Mater Chem
728 B*, 2023, doi: 10.1039/d2tb02447k.
- 729 [41] B. L. Wang, S. B. Kou, Z. Y. Lin, J. H. Shi, and Y. X. Liu, "Insights on the interaction
730 mechanism of brigatinib to human α -1-acid glycoprotein: Experimental and
731 computational approaches," *Int J Biol Macromol*, vol. 157, pp. 340–349, Aug. 2020,
732 doi: 10.1016/J.IJBIOMAC.2020.04.151.
- 733 [42] B. L. Wang, S. B. Kou, Z. Y. Lin, and J. H. Shi, "Insight into the binding behavior of
734 ceritinib on human α -1 acid glycoprotein: Multi-spectroscopic and molecular
735 modeling approaches," *Spectrochim Acta A Mol Biomol Spectrosc*, vol. 232, p. 118160,
736 May 2020, doi: 10.1016/J.SAA.2020.118160.
- 737 [43] N. Farajzadeh-Dehkordi, S. Farhadian, Z. Zahraei, S. Asgharzadeh, B. Shareghi, and B.
738 Shakerian, "Insights into the binding interaction of Reactive Yellow 145 with human
739 serum albumin from a biophysics point of view," *J Mol Liq*, vol. 369, p. 120800, Jan.
740 2023, doi: 10.1016/J.MOLLIQ.2022.120800.
- 741 [44] S. Hazra and G. Suresh Kumar, "Structural and thermodynamic studies on the
742 interaction of iminium and alkanolamine forms of sanguinarine with hemoglobin,"
743 *Journal of Physical Chemistry B*, vol. 118, no. 14, pp. 3771–3784, Apr. 2014, doi:
744 10.1021/jp409764z.
- 745 [45] B. Alpert, D. M. Jameson, and G. Weber, "TRYPTOPHAN EMISSION FROM HUMAN
746 HEMOGLOBIN AND ITS ISOLATED SUBUNITS," *Photochem Photobiol*, vol. 31, no. 1, pp.
747 1–4, 1980, doi: 10.1111/j.1751-1097.1980.tb03674.x.
- 748 [46] B. L. Wang, D. Q. Pan, K. L. Zhou, Y. Y. Lou, and J. H. Shi, "Multi-spectroscopic
749 approaches and molecular simulation research of the intermolecular interaction
750 between the angiotensin-converting enzyme inhibitor (ACE inhibitor) benazepril and
751 bovine serum albumin (BSA)," *Spectrochim Acta A Mol Biomol Spectrosc*, vol. 212, pp.
752 15–24, Apr. 2019, doi: 10.1016/j.saa.2018.12.040.
- 753 [47] Y. F. Zhang, K. L. Zhou, Y. Y. Lou, D. Q. Pan, and J. H. Shi, "Investigation of the binding
754 interaction between estazolam and bovine serum albumin: Multi-spectroscopic
755 methods and molecular docking technique," Dec. 21, 2017, *Taylor and Francis Ltd.*
756 doi: 10.1080/07391102.2016.1264889.

- 757 [48] Q. Wang *et al.*, "Binding interaction of atorvastatin with bovine serum albumin:
758 Spectroscopic methods and molecular docking," *Spectrochim Acta A Mol Biomol*
759 *Spectrosc*, vol. 156, pp. 155–163, Mar. 2016, doi: 10.1016/j.saa.2015.12.003.
- 760 [49] S. B. Corchnoy, T. E. Swartz, J. W. Lewis, I. Szundi, W. R. Briggs, and R. A. Bogomolni,
761 "Intramolecular proton transfers and structural changes during the photocycle of the
762 LOV2 domain of phototropin 1," *Journal of Biological Chemistry*, vol. 278, no. 2, pp.
763 724–731, Jan. 2003, doi: 10.1074/jbc.M209119200.
- 764 [50] H. Chugh, P. Kumar, N. Kumar, R. K. Gaur, G. Dhawan, and R. Chandra, "Ex vivo binding
765 studies of the anti-cancer drug noscapine with human hemoglobin: a spectroscopic
766 and molecular docking study," *New Journal of Chemistry*, vol. 45, no. 3, pp. 1525–
767 1534, Jan. 2021, doi: 10.1039/D0NJ03334K.
- 768 [51] A. Manna and S. Chakravorti, "Role of block copolymer-micelle nanocomposites in
769 dye-bovine serum albumin binding: A combined experimental and molecular docking
770 study," *Mol Biosyst*, vol. 9, no. 2, pp. 246–257, Feb. 2013, doi: 10.1039/c2mb25368b.
- 771 [52] J. Q. Tong *et al.*, "Probing the adverse temperature dependence in the static
772 fluorescence quenching of BSA induced by a novel anticancer hydrazone,"
773 *Photochemical and Photobiological Sciences*, vol. 11, no. 12, pp. 1868–1879, 2012,
774 doi: 10.1039/c2pp25162k.
- 775 [53] F. F. Tian *et al.*, "The adsorption of an anticancer hydrazone by protein: An unusual
776 static quenching mechanism," *RSC Adv*, vol. 2, no. 2, pp. 501–513, Jan. 2012, doi:
777 10.1039/c1ra00521a.
- 778 [54] F. F. Tian *et al.*, "Synthesis of a novel hydrazone derivative and biophysical studies of
779 its interactions with bovine serum albumin by spectroscopic, electrochemical, and
780 molecular docking methods," *Journal of Physical Chemistry B*, vol. 114, no. 46, pp.
781 14842–14853, Nov. 2010, doi: 10.1021/jp105766n.
- 782 [55] M. Bagheri and M. H. Fatemi, "Fluorescence spectroscopy, molecular docking and
783 molecular dynamic simulation studies of HSA-Aflatoxin B1 and G1 interactions," *J*
784 *Lumin*, vol. 202, 2018, doi: 10.1016/j.jlumin.2018.05.066.
- 785 [56] Y. Z. Zhang, B. Zhou, X. P. Zhang, P. Huang, C. H. Li, and Y. Liu, "Interaction of malachite
786 green with bovine serum albumin: Determination of the binding mechanism and
787 binding site by spectroscopic methods," *J Hazard Mater*, vol. 163, no. 2–3, 2009, doi:
788 10.1016/j.jhazmat.2008.07.132.
- 789 [57] N. Shahabadi, S. Hadidi, Z. Abdoli, and Z. Mardani, "Interaction of a cobalt(III) complex
790 containing β -amino alcohol with human serum albumin (HSA): Spectroscopic and
791 molecular docking methods," *J Mol Liq*, vol. 384, 2023, doi:
792 10.1016/j.molliq.2023.122187.
- 793 [58] A. Mavani, D. Ray, V. K. Aswal, and J. Bhattacharyya, "Understanding the molecular
794 interaction of BSA protein with antibiotic sulfa molecule(s) for novel drug
795 development," *J Mol Struct*, vol. 1287, 2023, doi: 10.1016/j.molstruc.2023.135697.
- 796 [59] J. F. Thériault, L. Yu, P. Stephen, Y. Sheng, and S. X. Lin, "Tunable ultraviolet laser
797 induces high signal-to-noise ratio in intrinsic fluorescence titration for protein- ligand
798 interaction studies," *Results Phys*, vol. 44, p. 106120, Jan. 2023, doi:
799 10.1016/J.RINP.2022.106120.
- 800 [60] M. Alrouji, F. A. Alhumaydhi, K. Venkatesan, S. E. Sharaf, M. Shahwan, and A. Shamsi,
801 "Evaluation of binding mechanism of dietary phytochemical, capsaicin, with human
802 transferrin: targeting neurodegenerative diseases therapeutics," *Front Pharmacol*, vol.
803 15, pp. 1–9, 2024, doi: 10.3389/FPHAR.2024.1348128/FULL.

- 804 [61] N. Gooran and K. Kopra, "Fluorescence-Based Protein Stability Monitoring-A Review,"
805 *Int J Mol Sci*, vol. 2024, p. 1764, 2024, doi: 10.3390/ijms25031764.
- 806 [62] R. Dudure, R. Joshi, P. Pritam, A. K. Panda, and M. Jadhao, "Probing the interaction
807 and aggregation of lysozyme in presence of organophosphate pesticides: a
808 comprehensive spectroscopic, calorimetric, and in-silico investigation," *J Biomol Struct
809 Dyn*, pp. 1–15, 2023, doi: 10.1080/07391102.2023.2259484.
- 810 [63] J. Saraswat, S. Kumar, K. A. Alzahrani, M. A. Malik, and R. Patel, "Experimental and
811 Computational Characterisation of the Molecular Interactions between 1-Butyl-1-
812 methyl-pyrrolidin-1-ium bis(trifluoromethanesulphonyl)imide and Human Serum
813 Albumin," *ChemistrySelect*, vol. 8, no. 1, 2023, doi: 10.1002/slct.202204159.
- 814 [64] M. Esmaelpourfarkhani, M. Ramezani, M. Alibolandi, K. Abnous, and S. M. Taghdisi,
815 "Time-resolved Fluorescence DNA-based Sensors for Reducing Background
816 Fluorescence of Environment," 2023. doi: 10.1007/s10895-023-03239-7.
- 817 [65] H. Hosaka, R. Haruki, K. Yamada, C. B. Tchier, and T. Komatsu, "Hemoglobin–Albumin
818 Cluster Incorporating a Pt Nanoparticle: Artificial O₂ Carrier with Antioxidant
819 Activities," *PLoS One*, vol. 9, no. 10, p. e110541, Oct. 2014, doi:
820 10.1371/JOURNAL.PONE.0110541.
- 821 [66] A. Sindhu, R. S. Varma, and P. Venkatesu, "Cholinium-Based Ionic Liquids Attenuate
822 the Amyloid Fibril Formation of Lysozyme: A Greener Concept of Antiamyloidogenic
823 Ionic Liquids," *ACS Sustain Chem Eng*, vol. 10, no. 28, 2022, doi:
824 10.1021/acssuschemeng.2c02963.
- 825 [67] S. Joshi, A. Singh, and S. Kukreti, "Porphyrin induced structural destabilization of a
826 parallel DNA G-quadruplex in human MRP1 gene promoter," *Journal of Molecular
827 Recognition*, vol. 35, no. 3, 2022, doi: 10.1002/jmr.2950.
- 828 [68] A. Micsonai *et al.*, "BeStSel: Webserver for secondary structure and fold prediction for
829 protein CD spectroscopy," *Nucleic Acids Res*, vol. 50, no. W1, 2022, doi:
830 10.1093/nar/gkac345.
- 831 [69] A. Micsonai *et al.*, "Disordered–Ordered Protein Binary Classification by Circular
832 Dichroism Spectroscopy," *Front Mol Biosci*, vol. 9, 2022, doi:
833 10.3389/fmolb.2022.863141.
- 834 [70] J. A. Lukin, G. Kontaxis, V. Simplaceanu, Y. Yuan, A. Bax, and C. Ho, "Quaternary
835 structure of hemoglobin in solution," *Proc Natl Acad Sci U S A*, vol. 100, no. 2, 2003,
836 doi: 10.1073/pnas.232715799.
- 837 [71] I. D. Kuleshova *et al.*, "Changes in Hemoglobin Properties in Complex with Glutathione
838 and after Glutathionylation," *Int J Mol Sci*, vol. 24, no. 17, 2023, doi:
839 10.3390/ijms241713557.
- 840 [72] A. Precupas, A. Ruxandra Leonties, A. Neacsu, D. George Angelescu, and V. Tudor
841 Popa, "Bovine hemoglobin thermal stability in the presence of naringenin:
842 Calorimetric, spectroscopic and molecular modeling studies," *J Mol Liq*, vol. 361,
843 2022, doi: 10.1016/j.molliq.2022.119617.
- 844 [73] M. Babu Singh, Himani, S. Yadav, and P. Singh, "A Theoretical Study To Understand the
845 Impact of Mpro of nCoV on the Hormones," *ChemistrySelect*, vol. 9, no. 8, p.
846 e202304767, Feb. 2024, doi: 10.1002/SLCT.202304767.
- 847 [74] M. B. Singh *et al.*, "An understanding of coronavirus and exploring the molecular
848 dynamics simulations to find promising candidates against the Mpro of nCoV to
849 combat the COVID-19: A systematic review," *J Infect Public Health*, vol. 15, no. 11, pp.
850 1326–1349, Nov. 2022, doi: 10.1016/J.JIPH.2022.10.013.

- 851 [75] T. Fukutani, K. Miyazawa, S. Iwata, and H. Satoh, "G-RMSD: Root Mean Square
852 Deviation Based Method for Three-Dimensional Molecular Similarity Determination,"
853 *Bull Chem Soc Jpn*, vol. 94, no. 2, pp. 655–665, Feb. 2021, doi:
854 10.1246/BCSJ.20200258.
- 855 [76] A. P. S. Raman *et al.*, "An investigation for the interaction of gamma oryzanol with the
856 Mpro of SARS-CoV-2 to combat COVID-19: DFT, molecular docking, ADME and
857 molecular dynamics simulations," *J Biomol Struct Dyn*, vol. 41, no. 5, pp. 1919–1929,
858 2023, doi: 10.1080/07391102.2022.2029770.
- 859 [77] M. Mallick, T. R. Yoithap Prabhunath, S. Kumari, and M. E. Sobhia, "An in silico study of
860 protein-protein interactions and design of novel peptides for TrkA in ameloblastoma,"
861 *J Biomol Struct Dyn*, 2023, doi: 10.1080/07391102.2023.2278083.
- 862 [78] K. Sargsyan, C. Grauffel, and C. Lim, "How Molecular Size Impacts RMSD Applications
863 in Molecular Dynamics Simulations," *J Chem Theory Comput*, vol. 13, no. 4, pp. 1518–
864 1524, Apr. 2017, doi: 10.1021/ACS.JCTC.7B00028/ASSET/IMAGES/LARGE/CT-2017-
865 000289_0005.JPEG.
- 866 [79] D. J. Price and C. L. Brooks, "Modern protein force fields behave comparably in
867 molecular dynamics simulations," *J Comput Chem*, vol. 23, no. 11, pp. 1045–1057,
868 Aug. 2002, doi: 10.1002/JCC.10083.
- 869 [80] P. Singh, D. Kumar, S. Pal, K. Kumari, and I. Bahadur, "L-amino-acids as immunity
870 booster against COVID-19: DFT, molecular docking and MD simulations," *J Mol Struct*,
871 vol. 1250, p. 131924, Feb. 2022, doi: 10.1016/J.MOLSTRUC.2021.131924.
- 872 [81] J. Zhu, D. Shen, B. Jin, and S. Wu, "Theoretical investigation on the formation
873 mechanism of carbonate ion in microbial self-healing concrete: Combined QC
874 calculation and MD simulation," *Constr Build Mater*, vol. 342, p. 128000, Aug. 2022,
875 doi: 10.1016/J.CONBUILDMAT.2022.128000.
- 876 [82] M. Heinig and D. Frishman, "STRIDE: A web server for secondary structure assignment
877 from known atomic coordinates of proteins," *Nucleic Acids Res*, vol. 32, no. WEB
878 SERVER ISS., 2004, doi: 10.1093/nar/gkh429.
- 879 [83] V. Mishyn *et al.*, "'Click' Chemistry on Gold Electrodes Modified with Reduced
880 Graphene Oxide by Electrophoretic Deposition," *Surfaces*, vol. 2, no. 1, pp. 193–204,
881 Mar. 2019, doi: 10.3390/SURFACES2010015.
- 882 [84] N. Rasitanon, P. Rattanapan, K. Kaewpradub, C. Buranachai, and I. Jeerapan, "Glucose
883 Oxidase/Egg White Protein Microparticles with a Redox Mediator for Glucose
884 Biosensors on a Screen-Printed Electrode and a Decomposable Electrode," *Biosensors*
885 (*Basel*), vol. 13, no. 8, p. 772, Aug. 2023, doi: 10.3390/BIOS13080772/S1.
- 886 [85] H. Kivrak, K. Selcuk, A. Caglar, and N. Aktas, "Selective Electrochemical Determination
887 of L-Cysteine by a Cobalt Carbon Nanotube (CNT)-Modified Glassy Carbon Electrode
888 (GCE)," *Anal Lett*, 2024, doi: 10.1080/00032719.2024.2302398.
- 889 [86] O. van der Heijden, S. Park, R. E. Vos, J. J. J. Eggebeen, and M. T. M. Koper, "Tafel Slope
890 Plot as a Tool to Analyze Electrocatalytic Reactions," *ACS Energy Lett*, vol. 9, no. 4, pp.
891 1871–1879, Apr. 2024, doi:
892 10.1021/ACSENERGYLETT.4C00266/ASSET/IMAGES/LARGE/NZ4C00266_0004.JPEG.
893
894